

Remote gate control of topological transitions in moiré superlattices via cavity vacuum fields

Zuzhang Lin,^{1,2} Chengxin Xiao,^{1,2} Danh-Phuong Nguyen,³ Geva Arwas,³ Cristiano Ciuti,³ and Wang Yao^{1,2,*}

¹*Department of Physics, The University of Hong Kong, Hong Kong, China*

²*HKU-UCAS Joint Institute of Theoretical and Computational Physics at Hong Kong, China*

³*Université Paris Cité, CNRS, Matériaux et Phénomènes Quantiques, 75013 Paris, France*

(Dated: March 17, 2023)

Placed in cavity resonators with three-dimensionally confined electromagnetic wave, the interaction between quasiparticles in solids can be induced by exchanging virtual cavity photons, which can have a non-local characteristic. Here we investigate the possibility of utilizing this nonlocality to realize the remote control of the topological transition in mesoscopic moiré superlattices at full filling (one electron/hole per supercell) embedded in a split-ring terahertz electromagnetic resonator. We show that gate tuning one moiré superlattice can remotely drive a topological band inversion in another moiré superlattice not in contact but embedded in the same cavity. Our study of remote on/off switching of a topological transition provides a novel paradigm for the control of material properties via cavity vacuum fields.

In recent years, the strong interaction between light and condensed matter systems, typically realized in a cavity-embedded configuration, has attracted widespread research interest [1–15]. One of the most salient feature of this regime is that the exchange of virtual cavity photons can mediate a plethora of virtual-excitation-dressed ground states [16], including superconductivity [17, 18], superfluidity [19] and charge-density-wave phases [20]. Most importantly, the virtual-photon-mediated interaction can possess a remarkable nonlocal character when the cavity photon mode field is discretized in energy while delocalized all over the electronic sample, as it has been pioneered in the context of the quantum Hall effect [21–23].

The nonlocality raises the intriguing possibility of remote control of a matter system. However, this has been largely overlooked as most research efforts regard cavity-embedded matter as a macroscopic system in the thermodynamic limit [3, 8, 24–26]. To uncover the remote control possibilities from the nonlocal characteristic, one has to consider mesoscopic configurations. In this respect, an interesting configuration is mesoscopic moiré superlattice embedded in a metallic split-ring terahertz (THz) electromagnetic resonator [21–23, 27–32]. The THz resonator enjoys deep subwavelength mode confinement and strongly enhanced electric field vacuum fluctuations [30, 31]. moiré superlattice—a platform for tailoring versatile material properties—is suitable for exploring cavity control at frequency down to the THz range, given their meV scale mini-gaps tunable by twisting angles [33]. In experimental reality, these superlattices are mesoscopic with practically limited lattice sites, having spatial dimension much smaller than the cavity mode volume of the THz resonators. Most importantly, moiré superlattices exhibit remarkable topological matter properties [33–35] and can serve as a prototype for remote control of topological transitions in matters.

In this work, we demonstrate remote gate control of topological transition in a mesoscopic moiré superlattice (moiré 1), by gate tuning a second moiré superlattice (moiré 2) that shares the same cavity vacuum with moiré 1. Within a mean-field description corroborated by exact diagonalization calcu-

lations for smaller size system, we find that the presence of a moiré can perturb the cavity vacuum field, which, in turn, introduces a mass term to tune the topological transition of the moiré minibands. This forms the basis of the cavity-mediated nonlocal interaction between two moiré superlattices embedded in a common cavity. By tuning the interlayer bias applied on moiré 2, a remote control of the mini-bands Chern numbers of moiré 1 can be realized, and vice versa. We emphasize that the present mechanism does not require any electronic contact between the two moiré samples which can also have different sizes and characteristic parameters. The principle can be straightforwardly extended to enable non-local interplay between multiple mesoscopic systems of distinct natures.

We consider the configuration where moiré 1 and moiré 2 are embedded into a THz resonator (Fig. 1). As an exemplary demonstration, let us assume that both moiré systems are transition metal dichalcogenides (TMDs) homobilayers with small twisting angles from 0 degree (R-type). The low energy valence states of such moiré superlattice at the **K** (**K'**) valley can be described by a two-band tight-binding (TB) model, of complex amplitude next-nearest-neighbor hopping on hexagonal superlattice sites due to the real-space Berry connection from moiré patterns, essentially a Haldane model [33, 35]. Without losing the essence of the physics to be discussed, we only consider one valley for each moiré, as the remote control via the cavity vacuum is valley-independent by itself. In the basis of their Bloch eigenstates, \hat{H}_1 and \hat{H}_2 can be written as $\hat{H}_1 = \sum_{\mathbf{k}} (E_{g\mathbf{k}} \hat{c}_{g\mathbf{k}}^\dagger \hat{c}_{g\mathbf{k}} + E_{e\mathbf{k}} \hat{c}_{e\mathbf{k}}^\dagger \hat{c}_{e\mathbf{k}})$ and $\hat{H}_2 = \sum_{\mathbf{q}} (\mathcal{E}_{g\mathbf{q}} \hat{d}_{g\mathbf{q}}^\dagger \hat{d}_{g\mathbf{q}} + \mathcal{E}_{e\mathbf{q}} \hat{d}_{e\mathbf{q}}^\dagger \hat{d}_{e\mathbf{q}})$, where \hat{c}^\dagger (\hat{c}) and \hat{d}^\dagger (\hat{d}) are creation (annihilation) fermionic operators of the quasiparticles in moiré 1 and moiré 2, respectively. Note that E and \mathcal{E} are corresponding moiré mini-band energies. The subscripts g and e respectively refer to the lower and upper bands, while \mathbf{k} and \mathbf{q} are the wavevectors of moiré 1 and moiré 2, respectively. The interlayer bias applied to such moiré superlattice creates onsite energy difference between its two sublattices, which can tune the mini-bands dispersion and topology locally.

Let us now consider a single-mode cavity with a cavity field

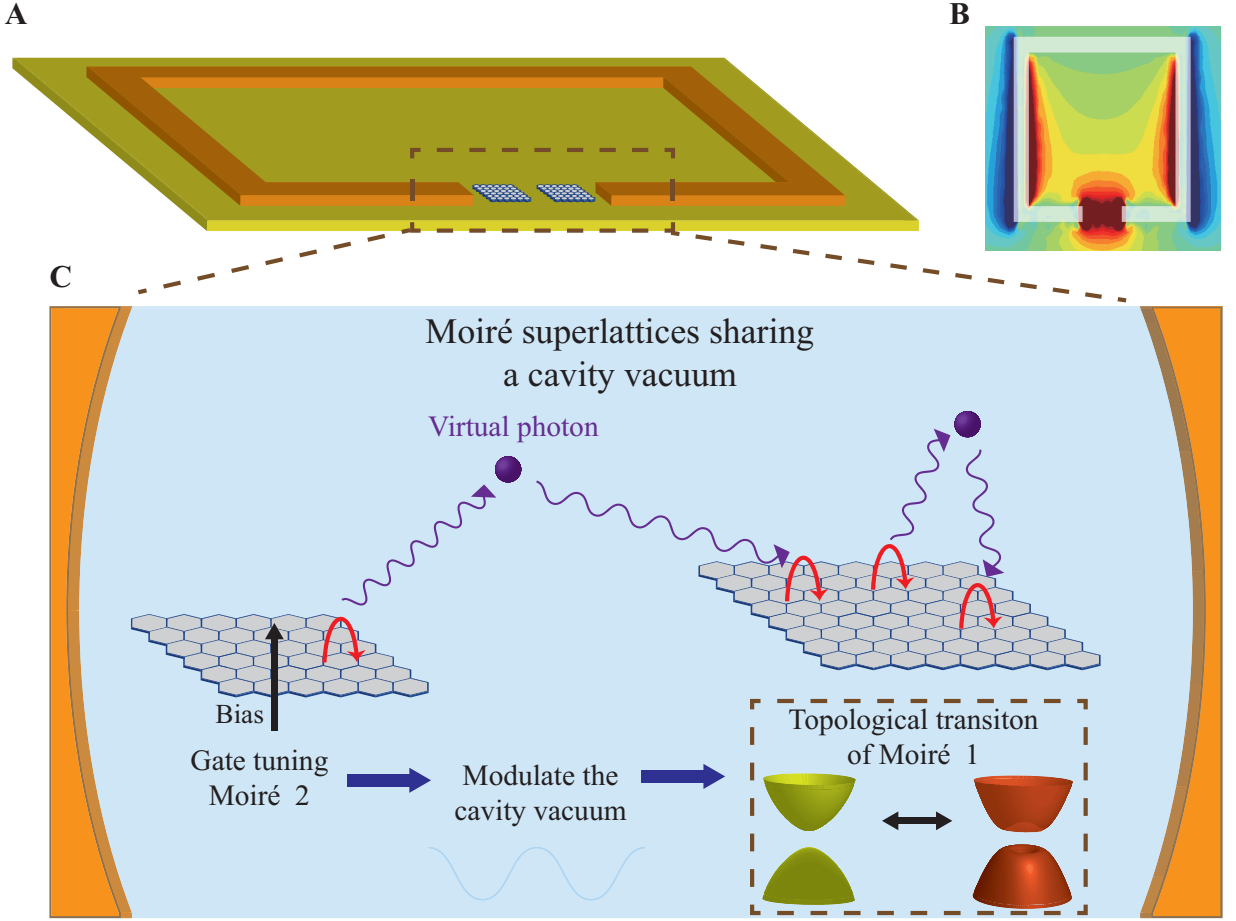


Figure 1. **Sketch of the remote topological control scheme via cavity vacuum fields.** (A) Set-up with two moiré superlattices (moiré 1 and moiré 2) embedded in a metallic split-ring THz electromagnetic resonator. (B) Schematic diagram of the spatial dependence of the cavity electric field concentrated on the gap of the metallic split-ring THz electromagnetic resonator (the red color denotes the part with the largest electric vacuum field). (C) Illustration of the physical mechanism providing remote control of the topological transition via cavity vacuum fields. The two moiré superlattices sharing the same cavity vacuum interact by exchanging virtual photons. By gate tuning moiré 2, a topological transition is induced in moiré 1.

polarized along the plane of the moiré superlattices. Within the TB model of the moiré superlattices the cavity coupling is enforced via the Peierls substitution. In the following, we will consider the light-matter Hamiltonian:

$$\hat{H} = \hat{H}_1 + \hat{H}_2 + \hat{H}_{1v} + \hat{H}_{2v} + \hat{H}_f, \quad (1)$$

where $\hat{H}_f = \hbar\omega\hat{a}^\dagger\hat{a}$ is the bare cavity Hamiltonian with ω the frequency of the cavity mode and \hbar the reduced Planck constant. The operator $\hat{H}_{1v} = \chi(a + a^\dagger)\hat{\mathcal{M}}$ ($\hat{H}_{2v} = \chi(a + a^\dagger)\hat{\mathcal{N}}$) describes the interaction between the cavity quantized field and moiré 1 (moiré 2), χ is the coupling strength, and $\hat{\mathcal{M}} \equiv \sum_{f,i\mathbf{k}} \mathcal{M}_{fi\mathbf{k}} \hat{c}_{f\mathbf{k}}^\dagger \hat{c}_{i\mathbf{k}}$ ($\hat{\mathcal{N}} \equiv \sum_{f,i\mathbf{q}} \mathcal{N}_{fi\mathbf{q}} \hat{d}_{f\mathbf{q}}^\dagger \hat{d}_{i\mathbf{q}}$) is a Hermitian operator with $i, f = g, e$.

The Hamiltonian \hat{H} acts on a Hilbert space consisting of subspaces ξ_n ($n = 0, 1, 2, \dots$) in which the photon num-

ber is $\langle a^\dagger a \rangle = n$. Following the Schrieffer-Wolff (SW) transformation [36] to eliminate the light-matter interaction ($\hat{H}_{1v} + \hat{H}_{2v}$) to the first order, we get a block diagonalized Hamiltonian $\hat{H}_S = e^{\hat{S}} \hat{H} e^{-\hat{S}}$ with the generator \hat{S} satisfying $[\hat{S}, \hat{H}_1 + \hat{H}_2 + \hat{H}_f] = -(\hat{H}_{1v} + \hat{H}_{2v})$. Projecting the Hamiltonian \hat{H}_S into the low energy sector (see Supplementary Material) gives an effective many-body Hamiltonian $\hat{H}_{\text{tot, eff}} = \hat{H}_{1, \text{eff}} + \hat{H}_{2, \text{eff}} + \hat{I}_1 + \hat{I}_2$. While the first two terms $\hat{H}_{1, \text{eff}} = \hat{H}_1 + \frac{1}{2}[\hat{S}_1, \hat{H}_{1v}]$ and $\hat{H}_{2, \text{eff}} = \hat{H}_2 + \frac{1}{2}[\hat{S}_2, \hat{H}_{2v}]$ describe the interaction of quasiparticles respectively in moiré 1 and moiré 2, the remaining two terms $\hat{I}_1 = \frac{1}{2}[\hat{S}_1, \hat{H}_{2v}]$ and $\hat{I}_2 = \frac{1}{2}[\hat{S}_2, \hat{H}_{1v}]$ denote that the quasiparticles in moiré 1 interact with quasiparticles in moiré 2. The specific form of \hat{I}_1 is

$$\hat{I}_1 = \frac{\chi^2}{2} \sum_{f\mathbf{k}, f'\mathbf{q}} \left(\frac{\mathcal{M}_{f\mathbf{k}} \hat{c}_{f\mathbf{k}}^\dagger \hat{c}_{f'\mathbf{q}} \mathcal{N}_{f'\mathbf{q}} \hat{d}_{f'\mathbf{q}}^\dagger \hat{d}_{f\mathbf{k}}}{E_{f\mathbf{k}} - E_{f'\mathbf{q}} - \hbar\omega} - \frac{\mathcal{N}_{f'\mathbf{q}} \hat{d}_{f'\mathbf{q}}^\dagger \hat{d}_{f\mathbf{k}} \mathcal{M}_{f\mathbf{k}} \hat{c}_{f\mathbf{k}}^\dagger \hat{c}_{f'\mathbf{q}}}{E_{f\mathbf{k}} - E_{f'\mathbf{q}} + \hbar\omega} \right) \quad (2)$$

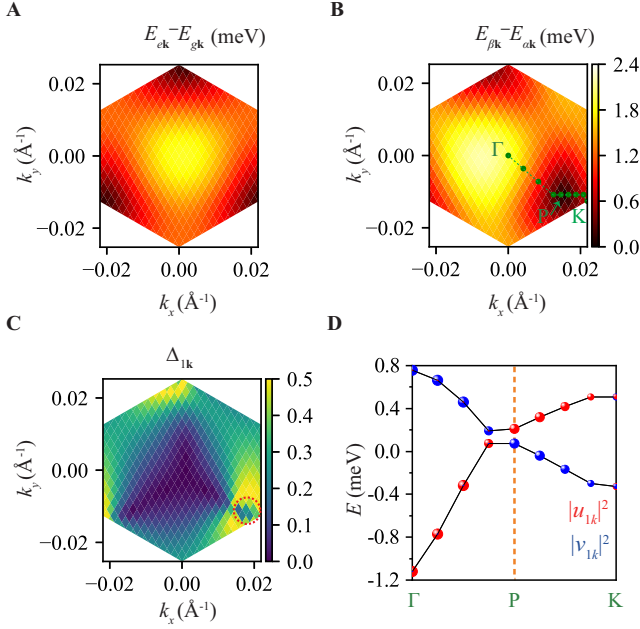


Figure 2. Inter-miniband transition energy, mean-field order parameter, and topological band inversion. (A-B) Color plot of the inter-miniband transition energy in reciprocal space for moiré 1 consisting of 21 by 21 superlattice sites. Calculation in (A) uses the bare Hamiltonian \hat{H}_1 , i.e. in the absence of cavity, and (B) uses $\hat{H}_{1,\text{MF}}$ in the presence of cavity quantized field perturbed by a second superlattice (moiré 2). See text. (C) Color plot of the mean-field order parameter $\Delta_{1\mathbf{k}}$ in reciprocal space, corresponding to the calculation in (B). (D) The miniband dispersion predicted by moiré 1's mean-field Hamiltonian $\hat{H}_{1,\text{MF}}$. The eigenstate amplitudes on to moiré 1's bare Hamiltonian basis are indicated by the size of the spheres.

Equation (2) indicates that the photons absorbed (emitted) during the transitions $|i\rangle \rightarrow |f\rangle$ of particles in moiré 1 will be emitted (absorbed) accompanying the transitions $|i'\rangle \rightarrow |f'\rangle$ of particles in moiré 2. These are the cavity-mediated interaction terms responsible for the remote control of moiré 2 on moiré 1, and vice versa. Note that for simplicity we have omitted the Coulomb electron-electron interaction terms in each moiré superlattice assuming that Coulomb interaction is strongly screened by a dielectric substrate. Regardless, the remote control scheme would remain the same with the cavity-mediated interaction between remote moiré superlattices.

Within a mean-field framework, we can approximate the bilinear terms in $\hat{H}_{\text{tot, eff}}$ as $\hat{O}\hat{O}' \approx \langle \hat{O} \rangle \hat{O}' + \hat{O} \langle \hat{O}' \rangle - \langle \hat{O} \rangle \langle \hat{O}' \rangle$, where $\hat{O}, \hat{O}' = \hat{c}_{f\mathbf{k}}^\dagger \hat{c}_{i\mathbf{k}}, \hat{d}_{f\mathbf{q}}^\dagger \hat{d}_{i\mathbf{q}}$. By grouping the resulting terms according to the operators $\hat{c}_{f\mathbf{k}}^\dagger \hat{c}_{i\mathbf{k}}$ and $\hat{d}_{f\mathbf{q}}^\dagger \hat{d}_{i\mathbf{q}}$, we get a mean-field Hamiltonian $\hat{H}_{\text{MF}} = \hat{H}_{1,\text{MF}} + \hat{H}_{2,\text{MF}}$, where

$\hat{H}_{1,\text{MF}}$ and $\hat{H}_{2,\text{MF}}$ respectively describe the mean-field effects on moiré 1 and moiré 2:

$$\begin{aligned} \hat{H}_{1,\text{MF}} &= \sum_{\mathbf{k}} [\tilde{E}_{g\mathbf{k}} \hat{c}_{g\mathbf{k}}^\dagger \hat{c}_{g\mathbf{k}} + \tilde{E}_{e\mathbf{k}} \hat{c}_{e\mathbf{k}}^\dagger \hat{c}_{e\mathbf{k}} + (\tilde{t}_{1\mathbf{k}} \hat{c}_{g\mathbf{k}}^\dagger \hat{c}_{e\mathbf{k}} + h.c.)] + \varepsilon_1, \\ \hat{H}_{2,\text{MF}} &= \sum_{\mathbf{q}} [\tilde{E}_{g\mathbf{q}} \hat{d}_{g\mathbf{q}}^\dagger \hat{d}_{g\mathbf{q}} + \tilde{E}_{e\mathbf{q}} \hat{d}_{e\mathbf{q}}^\dagger \hat{d}_{e\mathbf{q}} + (\tilde{t}_{2\mathbf{q}} \hat{d}_{g\mathbf{q}}^\dagger \hat{d}_{e\mathbf{q}} + h.c.)] + \varepsilon_2. \end{aligned} \quad (3)$$

Here $\tilde{E}_{g\mathbf{k}}, \tilde{E}_{e\mathbf{k}}, \tilde{t}_{1\mathbf{k}}, \tilde{E}_{g\mathbf{q}}, \tilde{E}_{e\mathbf{q}}, \tilde{t}_{2\mathbf{q}}, \varepsilon_1$ and ε_2 are renormalized parameters with mean-field corrections (see details in Supplementary Material). The many-body ground state $|\Psi\rangle = \prod_{\mathbf{k}} (u_{1\mathbf{k}}^* \hat{c}_{g\mathbf{k}}^\dagger + v_{1\mathbf{k}}^* \hat{c}_{e\mathbf{k}}^\dagger) \prod_{\mathbf{q}} (u_{2\mathbf{q}}^* \hat{d}_{g\mathbf{q}}^\dagger + v_{2\mathbf{q}}^* \hat{d}_{e\mathbf{q}}^\dagger) |0\rangle$ features interband coherence of moiré 1 (moiré 2) characterized by the mean-field order parameter $\Delta_{1\mathbf{k}} = v_{1\mathbf{k}} u_{1\mathbf{k}}^*$ ($\Delta_{2\mathbf{q}} = v_{2\mathbf{q}} u_{2\mathbf{q}}^*$). The mean-field order parameters can be solved self-consistently through the following gap-like equations

$$\begin{aligned} \Delta_{1\mathbf{k}} &= -\frac{\tilde{t}_{1\mathbf{k}}}{\sqrt{4|\tilde{t}_{1\mathbf{k}}|^2 + (\tilde{E}_{e\mathbf{k}} - \tilde{E}_{g\mathbf{k}})^2}}, \\ \Delta_{2\mathbf{q}} &= -\frac{\tilde{t}_{2\mathbf{q}}}{\sqrt{4|\tilde{t}_{2\mathbf{q}}|^2 + (\tilde{E}_{e\mathbf{q}} - \tilde{E}_{g\mathbf{q}})^2}}. \end{aligned} \quad (4)$$

Note that these two equations are not independent: the order parameters of moiré 1 are affected by the order parameters of moiré 2, and vice versa. To test the validity of our mean-field approach, we have also performed exact diagonalization results with a small number of electrons, yielding the same qualitative results (see the Supplementary Material).

In the calculations presented below, to exemplify the dissimilarities of the two moiré superlattices, we use a 21 by 21 superlattice for moiré 1 with strengths of the nearest and next-nearest neighbor hopping being 0.29 meV and 0.06 meV respectively [33], while moiré 2 is a 10 by 10 superlattice with the corresponding hopping amplitudes being 0.5 meV and 0.2 meV instead [35]. The phase of the next-nearest-hopping is $2\pi/3$ for both moirés, corresponding to a positive flux Haldane model from valley K. We consider a THz resonator cavity mode of volume $V = 7 \times 10^6 \text{ nm}^3$ and quantized mode energy $\hbar\omega = 8.1 \text{ meV}$, which leads to a light-matter coupling strength $\chi = 0.17$. More details are given in Supplementary Material.

As an example, we first solve the gap equation by fixing the interlayer bias applied on moiré 1 at 0.7 meV. In the absence of the cavity quantized field (i.e., $\chi = 0$), moiré 1 displays an electronic band gap at the K point (Fig. 2A) and is topologically trivial. Embedding moiré 1 alone in the cavity, we find negligible change is introduced to its electronic structure at the given bias, whereas the cavity vacuum is also negligibly

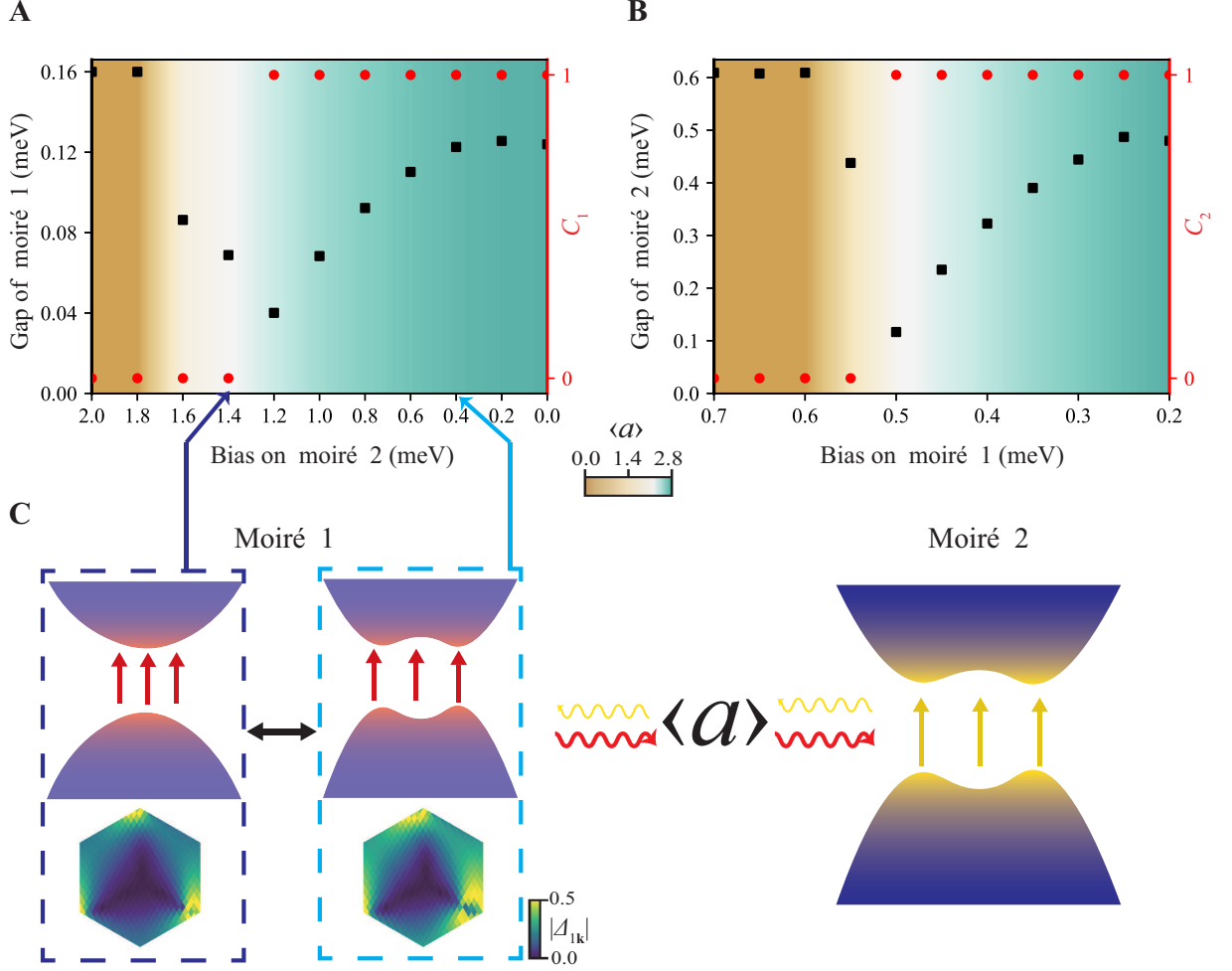


Figure 3. **Remote gate control of topological transitions.** (A) Topological transition of moiré 1 controlled remotely by the interlayer bias of moiré 2 (V_2), while fixing moiré 1's own bias at 0.7 meV. The change of cavity field $\langle a \rangle$, moiré 1's Chern number and gap as function of V_2 are shown respectively by the background color, red dots, black squares. (B) The reciprocal topological control of moiré 2 remotely by the interlayer bias of moiré 1 (V_1), while fixing moiré 2's bias at 2.2 meV. (C) Schematic diagram of the interaction due to the exchange of virtual photons between moiré 1 and moiré 2. At two V_2 values, the mean-field order parameter $\Delta_{1\mathbf{k}}$ is shown, where moiré 1 is topologically trivial and nontrivial respectively.

perturbed. When the cavity also hosts a second moiré, tuning the bias of moiré 2 can drastically change the electronic structure of moiré 1. In Fig. 2B, we plot the mini-band transition energies of moiré 1, calculated when moiré 2 is biased at 0.2 meV, which now exhibits an electronic band gap at the \mathbf{P} point instead. Its ground state has a pronounced interband coherence near the \mathbf{K} point (Fig. 2C), which is reasonable according to the Eq. (4) as $\tilde{\mathcal{E}}_{e\mathbf{k}} - \tilde{\mathcal{E}}_{g\mathbf{k}} \propto \mathcal{E}_{e\mathbf{k}} - \mathcal{E}_{g\mathbf{k}}$ reaches the smallest value near the \mathbf{K} point.

Notably, a small circular region (indicated by the red dashed circle in Fig. 2C) where $\Delta_{1\mathbf{k}}$ is almost zero, is surrounded by the areas with maximal interband coherence ($\Delta_{1\mathbf{k}} \sim 0.5$). We note that the zero $\Delta_{1\mathbf{k}}$ at this region is due to band inversion ($v_{1\mathbf{k}} = 1, u_{1\mathbf{k}} = 0$), which is different from the zero $\Delta_{1\mathbf{k}}$ elsewhere (e.g. in the region near Γ point where $v_{1\mathbf{k}} = 0, u_{1\mathbf{k}} = 1$). This is confirmed by the band dispersion of

the Hamiltonian $\hat{H}_{1,\text{MF}}$ and by the wavefunction projections on the original Hamiltonian basis (Fig. 2D). Furthermore, the calculated Chern numbers of the lower and upper bands are found to be 1 and -1, respectively. Therefore, in the presence of moiré 2, the cavity-mediated interaction has provided a topological nontrivial mass term to moiré 1.

This topological nontrivial mass term on moiré 1 arising from the cavity-mediated coupling is tunable by the interlayer bias on moiré 2. As a result, gate tuning moiré 2 will realize a remote control of the topological transition in moiré 1. By tuning the interlayer bias on moiré 2 (denoted as V_2 hereafter) from 2 meV to 0 meV, we indeed observe the gap of moiré 1 closes and reopens at a critical value of 1.2 meV of V_2 , accompanied by a corresponding step change in Chern number from zero to one (Fig. 3A). Conversely, the remote control of topological transition in moiré 2 by gate tuning moiré 1 (V_1)

can also be realized (Fig. 3B).

To reveal the physical insight of the remote control, we calculate the expectation value of field operator \hat{a} to the leading order

$$\langle a \rangle = \langle \Psi | e^{\hat{S}} \hat{a} e^{-\hat{S}} | \Psi \rangle$$

$$\sum_{fik} \frac{\chi \mathcal{M}_{fik} \langle \hat{c}_{fk} \hat{c}_{ik} \rangle}{E_{ik} - E_{fk} - \hbar\omega} + \sum_{fiq} \frac{\chi \mathcal{N}_{fiq} \langle \hat{d}_{fq} \hat{d}_{iq} \rangle}{\mathcal{E}_{iq} - \mathcal{E}_{fq} - \hbar\omega} \quad (5)$$

as a function of the interlayer bias. As shown in Fig. 3A, when V_2 is tuned from 2 meV to 1.8 meV, $\langle a \rangle$ is negligibly small and the gap of moiré 1 remains unchanged. Further reducing V_2 , $\langle a \rangle$ starts to increase noticeably, and at the same time the gap of moiré 1 starts to change, and eventually a topological transition occurs. Therefore, the remote control of topological transition in moiré 1 is realized through modulating the cavity vacuum upon gate tuning moiré 2. We find that nonzero $\langle a \rangle$ [37] occurs simultaneously with the interband coherence of the electronic many-body ground state. In parameter regimes where $\langle a \rangle$ vanishes, both moirés have negligible interband coherence in the ground states and have no response to the remote control gate. The threshold $\langle a \rangle$ value needed to bring a moiré across the topological transition point depends on the parameters of its bare Hamiltonian without the cavity (c.f. Fig. 3A and 3B).

We also notice that the light-matter coupling terms $\chi(\hat{a}^\dagger + \hat{a}) \sum_{\mathbf{k}} \mathcal{M}_{g\mathbf{k}} \hat{c}_{\mathbf{k}}^\dagger \hat{c}_{\mathbf{k}}$ and $\chi(\hat{a}^\dagger + \hat{a}) \sum_{\mathbf{q}} \mathcal{N}_{g\mathbf{q}} \hat{d}_{\mathbf{q}}^\dagger \hat{d}_{\mathbf{q}}$, which perturb the cavity vacuum while leaving the electronic state unaffected, are essential here. The nonzero value of $\mathcal{M}_{g\mathbf{k}}$ and $\mathcal{N}_{g\mathbf{q}}$ are allowed here by the lack of parity in eigenstates of Hamiltonians \hat{H}_1 and \hat{H}_2 as the out-of-plane mirror symmetry is broken in twisted TMDs bilayers. The expectation values $\langle \mathcal{M}_{g\mathbf{k}} \hat{c}_{\mathbf{k}}^\dagger \hat{c}_{\mathbf{k}} \rangle$ and $\langle \sum_{\mathbf{q}} \mathcal{N}_{g\mathbf{q}} \hat{d}_{\mathbf{q}}^\dagger \hat{d}_{\mathbf{q}} \rangle$ vanish in the ground states of the bare moiré Hamiltonians \hat{H}_1 and \hat{H}_2 respectively, but become finite in the ground states of their mean-field interaction Hamiltonian $\hat{H}_{1,\text{MF}}$ and $\hat{H}_{2,\text{MF}}$ under bias parameters where interband coherence spontaneously emerges.

In conclusion, we have shown that by gate tuning a remote moiré superlattice it is possible to induce a topological transition of a second mesoscopic moiré system via cavity vacuum field. The remote cascade control of multiple moiré superlattices embedded in one cavity is possible following the same scheme. Besides topological transitions, the mesoscopic system consisting of cavity-embedded moiré superlattices may also provide an exciting platform to investigate the possible remote control of other physical properties, such as superconductivity and ferromagnetism.

Acknowledgment: We thank Hsun-Chi Chan for helping us generate Fig. 1B. **Fundings:** The work is supported by Research Grant Council (RGC) of Hong Kong SAR China through grants HKU SRFS2122-7S05 and AoE/P-701/20, and a grant under the ANR/RGC Joint Research Scheme sponsored by RGC and French National Research Agency (A-HKU705/21, ANR-21-CE30-0056-01). W.Y. also acknowledges support by Tencent Foundation. G.A. and C.C. also

acknowledge support from the Israeli Council for Higher Education - VATAT. **Data and materials availability:** All data needed to evaluate the conclusions in the paper are present in the paper and/or the Supplementary Materials. All data related to this study may be available from the corresponding author upon reasonable request.

* wangyao@hku.hk

- [1] F. J. Garcia-Vidal, C. Ciuti, and T. W. Ebbesen, Manipulating matter by strong coupling to vacuum fields, *Science* **373**, eabd0336 (2021).
- [2] M. A. Sentef, M. Ruggenthaler, and A. Rubio, Cavity quantum-electrodynamical polaritonically enhanced electron-phonon coupling and its influence on superconductivity, *Sci. Adv.* **4**, eaau6969 (2018).
- [3] G. Mazza and A. Georges, Superradiant Quantum Materials, *Phys. Rev. Lett.* **122**, 017401 (2019).
- [4] M. Kiffner, J. Coulthard, F. Schlawin, A. Ardavan, and D. Jaksch, Mott polaritons in cavity-coupled quantum materials, *New J. Phys.* **21**, 073066 (2019).
- [5] J. B. Curtis, Z. M. Raines, A. A. Allocca, M. Hafezi, and V. M. Galitski, Cavity Quantum Eliashberg Enhancement of Superconductivity, *Phys. Rev. Lett.* **122**, 167002 (2019).
- [6] A. A. Allocca, Z. M. Raines, J. B. Curtis, and V. M. Galitski, Cavity superconductor-polaritons, *Phys. Rev. B* **99**, 020504 (2019).
- [7] S. Latini, E. Ronca, U. De Giovannini, H. Hübener, and A. Rubio, Cavity Control of Excitons in Two-Dimensional Materials, *Nano Lett.* **19**, 3473 (2019).
- [8] S. Latini, D. Shin, S. A. Sato, C. Schäfer, U. De Giovannini, H. Hübener, and A. Rubio, The ferroelectric photo ground state of SrTiO₃: Cavity materials engineering, *Proc. Natl. Acad. Sci.* **118**, e2105618118 (2021).
- [9] K. Lenk, J. Li, P. Werner, and M. Eckstein, Dynamical mean-field study of a photon-mediated ferroelectric phase transition, *Phys. Rev. B* **106**, 245124 (2022).
- [10] Ö. O. Soykal and M. E. Flatté, Strong Field Interactions between a Nanomagnet and a Photonic Cavity, *Phys. Rev. Lett.* **104**, 077202 (2010).
- [11] M. Cirio, S. De Liberato, N. Lambert, and F. Nori, Ground state electroluminescence, *Phys. Rev. Lett.* **116**, 113601 (2016).
- [12] R. Stassi, A. Ridolfo, O. Di Stefano, M. Hartmann, and S. Savasta, Spontaneous conversion from virtual to real photons in the ultrastrong-coupling regime, *Phys. Rev. Lett.* **110**, 243601 (2013).
- [13] O. Di Stefano, A. Settineri, V. Macrì, A. Ridolfo, R. Stassi, A. F. Kockum, S. Savasta, and F. Nori, Interaction of mechanical oscillators mediated by the exchange of virtual photon pairs, *Phys. Rev. Lett.* **122**, 030402 (2019).
- [14] P. Forn-Díaz, L. Lamata, E. Rico, J. Kono, and E. Solano, Ultrastrong coupling regimes of light-matter interaction, *Rev. Mod. Phys.* **91**, 025005 (2019).
- [15] Y. Ashida, A. Imamoglu, and E. Demler, Cavity quantum electrodynamics with hyperbolic van der Waals materials, arXiv preprint arXiv:2301.03712 (2023).
- [16] A. Frisk Kockum, A. Miranowicz, S. De Liberato, S. Savasta, and F. Nori, Ultrastrong coupling between light and matter, *Nat. Rev. Phys.* **1**, 19 (2019).
- [17] F. Schlawin, A. Cavalleri, and D. Jaksch, Cavity-Mediated Electron-Photon Superconductivity,

- Phys. Rev. Lett. **122**, 133602 (2019).
- [18] H. Gao, F. Schlawin, M. Buzzi, A. Cavalleri, and D. Jaksch, Photoinduced Electron Pairing in a Driven Cavity, *Phys. Rev. Lett.* **125**, 053602 (2020).
 - [19] F. Schlawin and D. Jaksch, Cavity-Mediated Unconventional Pairing in Ultracold Fermionic Atoms, *Phys. Rev. Lett.* **123**, 133601 (2019).
 - [20] J. Li and M. Eckstein, Manipulating Intertwined Orders in Solids with Quantum Light, *Phys. Rev. Lett.* **125**, 217402 (2020).
 - [21] C. Ciuti, Cavity-mediated electron hopping in disordered quantum hall systems, *Phys. Rev. B* **104**, 155307 (2021).
 - [22] F. Appugliese, J. Enkner, G. L. Paravicini-Bagliani, M. Beck, C. Reichl, W. Wegscheider, G. Scalari, C. Ciuti, and J. Faist, Breakdown of topological protection by cavity vacuum fields in the integer quantum hall effect, *Science* **375**, 1030 (2022).
 - [23] G. Arwas and C. Ciuti, Quantum electron transport controlled by cavity vacuum fields, *Phys. Rev. B* **107**, 045425 (2023).
 - [24] X. Li, M. Bamba, Q. Zhang, S. Fallahi, G. C. Gardner, W. Gao, M. Lou, K. Yoshioka, M. J. Manfra, and J. Kono, Vacuum Bloch-Siegert shift in Landau polaritons with ultra-high cooperativity, *Nat. Photonics* **12**, 324 (2018).
 - [25] G. M. Andolina, F. M. D. Pellegrino, V. Giovannetti, A. H. MacDonald, and M. Polini, Theory of photon condensation in a spatially varying electromagnetic field, *Phys. Rev. B* **102**, 125137 (2020).
 - [26] G. M. Andolina, F. M. D. Pellegrino, V. Giovannetti, A. H. MacDonald, and M. Polini, Cavity quantum electrodynamics of strongly correlated electron systems: A no-go theorem for photon condensation, *Phys. Rev. B* **100**, 121109 (2019).
 - [27] G. Scalari, C. Maissen, D. Turčinková, D. Hagenmüller, S. De Liberato, C. Ciuti, C. Reichl, D. Schuh, W. Wegscheider, M. Beck, and J. Faist, Ultrastrong Coupling of the Cyclotron Transition of a 2D Electron Gas to a THz Metamaterial, *Science* **335**, 1323 (2012).
 - [28] H.-T. Chen, A. J. Taylor, and N. Yu, A review of metasurfaces: physics and applications, *Rep. Prog. Phys.*, 41 (2016).
 - [29] G. L. Paravicini-Bagliani, G. Scalari, F. Valmorra, J. Keller, C. Maissen, M. Beck, and J. Faist, Gate and magnetic field tunable ultrastrong coupling between a magnetoplasmon and the optical mode of an LC cavity, *Phys. Rev. B* **95**, 205304 (2017).
 - [30] G. L. Paravicini-Bagliani, F. Appugliese, E. Richter, F. Valmorra, J. Keller, M. Beck, N. Bartolo, C. Rössler, T. Ihn, K. Ensslin, C. Ciuti, G. Scalari, and J. Faist, Magneto-transport controlled by Landau polariton states, *Nat. Phys.* **15**, 186 (2019).
 - [31] J. Keller, G. Scalari, S. Cibella, C. Maissen, F. Appugliese, E. Giovine, R. Leoni, M. Beck, and J. Faist, Few-Electron Ultrastrong Light-Matter Coupling at 300 GHz with Nanogap Hybrid LC Microcavities, *Nano Lett.* **17**, 7410 (2017).
 - [32] M. Jeannin, G. Mariotti Nesurini, S. Suffit, D. Gacemi, A. Vasanelli, L. Li, A. G. Davies, E. Linfield, C. Sirtori, and Y. Todorov, Ultrastrong Light-Matter Coupling in Deeply Subwavelength THz LC Resonators, *ACS Photonics* **6**, 1207 (2019).
 - [33] F. Wu, T. Lovorn, E. Tutuc, I. Martin, and A. MacDonald, Topological insulators in twisted transition metal dichalcogenide homobilayers, *Phys. Rev. Lett.* **122**, 086402 (2019).
 - [34] Q. Tong, H. Yu, Q. Zhu, Y. Wang, X. Xu, and W. Yao, Topological mosaics in moiré superlattices of van der waals heterobilayers, *Nat. Phys.* **13**, 356 (2017).
 - [35] H. Yu, M. Chen, and W. Yao, Giant magnetic field from moiré induced Berry phase in homobilayer semiconductors, *Natl. Sci. Rev.* **7**, 12 (2020).
 - [36] J. R. Schrieffer and P. A. Wolff, Relation between the anderson and kondo hamiltonians, *Phys. Rev.* **149**, 491 (1966).
 - [37] The nonzero mean values of the field operator \hat{a} does not imply a macroscopic photon condensation prevented by the no-go theorem [26, 38–41]. The moiré superlattices embedded in a metallic split-ring THz resonator form a mesoscopic system, where both the superlattice size and cavity volume are finite. In the literature convention [3, 8, 24–26], the field amplitude $A_0 \propto 1/\sqrt{\mathcal{V}}$ (\mathcal{V} the mode volume of the cavity photon) is infinitesimal in the thermodynamic limit in which \mathcal{V} is assigned to be infinite.
 - [38] D. Guerci, P. Simon, and C. Mora, Superradiant Phase Transition in Electronic Systems and Emergent Topological Phases, *Phys. Rev. Lett.* **125**, 257604 (2020).
 - [39] K. Rzażewski, K. Wódkiewicz, and W. Żakowicz, Phase Transitions, Two-Level Atoms, and the A^2 Term, *Phys. Rev. Lett.* **35**, 432 (1975).
 - [40] I. Bialynicki-Birula and K. Rzażewski, No-go theorem concerning the superradiant phase transition in atomic systems, *Phys. Rev. A* **19**, 301 (1979).
 - [41] K. Gawędzki and K. Rzażewski, No-go theorem for the superradiant phase transition without dipole approximation, *Phys. Rev. A* **23**, 2134 (1981).